


Tripartite entanglement and tripartite steering in three-qubit pure states induced by vacuum–one-photon superpositions

Jian Wang, Huan Liu, Xue-feng Zhan, and Xue-xiang Xu ^{*}*College of Physics and Communication Electronics, Jiangxi Normal University, Nanchang 330022, China*

(Received 27 January 2024; accepted 7 August 2024; published 26 August 2024)

Utilizing a tritter with variable parameter T and induced by vacuum–one-photon superpositions $|0\rangle + \alpha|1\rangle$ with $\alpha = |\alpha|e^{i\phi}$, we propose a scheme to prepare a class of three-qubit pure states. These states take the form of $|\psi\rangle_{123} = c_0|000\rangle + c_1|100\rangle + c_2|010\rangle + c_3|001\rangle$. The coefficients (c_0 , c_1 , c_2 , and c_3) can be manipulated through interaction parameters ($|\alpha|$, ϕ , and T). In line with Xie and Eberly’s work [*Phys. Rev. Lett.* **127**, 040403 (2021)], we investigate the genuine tripartite entanglement for $|\psi\rangle_{123}$ by using the measure of concurrence fill. Drawing on Hao *et al.*’s research [*Phys. Rev. Lett.* **128**, 120402 (2022)], we examine tripartite steering for $|\psi\rangle_{123}$ under certain measurements based on the uncertainty relations criterion. We identify nine potential configurations exhibiting varying steerability across different parameter spaces. It is important to highlight that, while the state $|\psi\rangle_{123}$ exhibits entanglement, steering remains unattainable in a substantial portion of the parameter space.

DOI: [10.1103/PhysRevA.110.022437](https://doi.org/10.1103/PhysRevA.110.022437)

I. INTRODUCTION

Entanglement is a key feature of quantum mechanics and plays an important role in many quantum information protocols [1–3], including quantum computation [4], quantum communication [5], and quantum metrology [6]. Previously, people paid more attention to studying bipartite entanglement in two-party systems. To quantify the amount of entanglement, they invented and developed a variety of entanglement measures, including partial-norm [7], entanglement of formation [8], von Neumann entropy [9], normalized negativity [10], concurrence [11], and so on. With the development of quantum technologies, more and more researchers began to study multipartite entanglement (ME), existing in three-party or even more-party systems. In general, ME can be divided as partial ME and “genuine” ME (GME). If a multipartite state can be at least biseparable, then it is a partial ME but not a GME [12].

GME is crucial for quantum information and quantum technologies [13]. In general, a GME measure necessitates the following five requirements [14,15]: (R1) It must assign the zero value to any product state or biseparate state; (R2) It must assign a positive value to all nonbiseparate states; (R3) It is convex; (R4) It is nonincreasing under local operations and classical communication (LOCC); and (R5) It is invariant under local unitary transformation. However, quantifying GME is still a challenge [16] because most existing measures do not meet the “genuine” requirements. For example, some measures, such as Schmidt measure by Eisert and Briegel [17], or global entanglement by Meyer and Wallach [18], will violate (R1). While other measures, like the three-tangle by Coffman *et al.* [19], or a generalized form of negativity by Junnitsch *et al.* [20], will violate (R2).

Recently, Xie and Eberly introduced a novel measure of genuine tripartite entanglement (called “concurrence fill”), which was defined as the square root of the area of concurrence triangle, multiplying a constant factor [21]. However, through a counterexample, Ge *et al.* pointed out that concurrence fill was a genuine entanglement measure, but not an entanglement monotone [22]. Afterwards, they presented several faithful geometric measures for GME [23].

Einstein-Podolsky-Rosen (EPR) steering [24,25], which stipulates that one observer can manipulate another party’s state through local measurements, is a crucial resource for various quantum applications [26]. Typically, two methods are employed to explore multipartite steering: the one-sided device-independent scenario [27] and the steering correlation between bipartitions [28,29]. Key areas of studying multipartite EPR steering include the monogamy [30–33] and the shareability [34]. Monogamy suggests that two observers cannot simultaneously steer the state of a third party, while the shareability implies that two observers can simultaneously steer a third observer. Over recent years, the monogamous aspects of EPR steering have garnered significant attention in both theoretical and experimental studies [32]. To circumvent monogamous relationships or eliminate monogamy constraints, researchers have uncovered additional configurations of multipartite EPR steering by expanding the number of measurement settings [35]. Paul and Mukherjee recently introduced explicit shareability relations using the violation of linear steering inequality [36]. Additionally, Hao *et al.* experimentally demonstrated various configurations of EPR steering shareability using a three-qubit system [37].

Entanglement and steering, as resources, are pivotal in various quantum protocols. A critical prerequisite is the distribution of these quantum resources among multiple remote users within a network [38,39]. Numerous multiqubit states, such as the two-qubit EPR state $(|10\rangle + |01\rangle)/\sqrt{2}$ [40], three-qubit GHZ state $|\text{GHZ}\rangle = (|000\rangle + |111\rangle)/\sqrt{2}$ [41], and

^{*}Contact author: xuxuexiang@jxnu.edu.cn

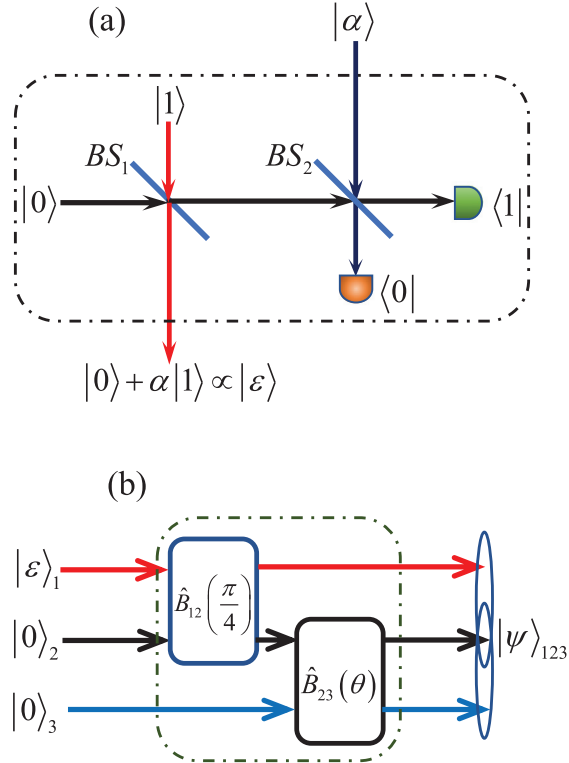


FIG. 1. (a) The preparation of the VOPS $|0\rangle + \alpha|1\rangle \propto |\varepsilon\rangle$ is achieved utilizing a QS device. This QS operation consists of two BSs. (b) The preparation of the three-qubit state $|\psi\rangle_{123}$ is executed using a tritter

three-qubit W state $|W\rangle = (|100\rangle + |010\rangle + |001\rangle)/\sqrt{3}$ [42] have been extensively examined by assessing their potential entanglement and steering [43,44] for suitable applications. In this study, we will introduce a class of three-qubit states and analyze their tripartite entanglement and steering.

The paper is structured as follows. In Sec. II, we propose a scheme to prepare a class of three-qubit pure states. In Sec. III, we explore “genuine” tripartite entanglement by using the measure of concurrence. Section IV delves into tripartite steering based on the uncertainty relations criterion under specific measurement settings. Finally, Sec. V encapsulates the primary findings.

II. PREPARATION OF THREE-QUBIT PURE STATES

In this section, we propose a scheme to prepare a class of three-qubit pure states. As shown in Fig. 1, we divide the entire process into the following two stages.

A. Stage 1: Preparation of the vacuum–one-photon superposition

As proposed by Pegg, Phillips, and Barnett [45], the vacuum–one-photon superposition (VOPS) $|0\rangle + \alpha|1\rangle$ can be prepared by utilizing a quantum scissor (QS) device. The conceptual scheme is shown in Fig. 1(a). The input coherent state $|\alpha\rangle$ is mixed on a balanced BS_2 with an ancillary signal, and both outputs are measured using two single-photon detectors. The ancillary signal is one of the two outputs of a single

photon passing another balanced BS_1 , while the other signal is the output VOPS. Of course, successful operation is heralded when a single photon is detected at one detector and none at the other detector with perfect manner [46]. It is important to note that this VOPS is truncated from the input coherent state $|\alpha\rangle$ (by setting $\alpha = |\alpha|e^{i\phi}$) and will subsequently be normalized as $|\varepsilon\rangle = \omega_0|0\rangle + \omega_1|1\rangle$ with $\omega_0 = 1/\sqrt{1 + |\alpha|^2}$ and $\omega_1 = \alpha/\sqrt{1 + |\alpha|^2}$. Very recently, Miranowicz *et al.* explored the nonclassicality of the VOPSs [47]. In addition, the prepared VOPS will serve as one of the input states of stage 2.

B. Stage 2: Preparation of the three-qubit states under study

As depicted in Fig. 1(b), the kernel device is referred to as a tritter [48,49] comprised of two consecutive BSs. We postulate the following: (i) the initial BS is characterized by $\hat{B}_{12}(\pi/4) = e^{-\frac{\pi}{4}(\hat{a}_1^\dagger \hat{a}_2 - \hat{a}_1 \hat{a}_2^\dagger)}$, satisfying $\hat{B}_{12} \hat{a}_1^\dagger \hat{B}_{12}^\dagger = \frac{1}{\sqrt{2}} \hat{a}_1^\dagger - \frac{1}{\sqrt{2}} \hat{a}_2^\dagger$ and $\hat{B}_{12} \hat{a}_2^\dagger \hat{B}_{12}^\dagger = \frac{1}{\sqrt{2}} \hat{a}_1^\dagger + \frac{1}{\sqrt{2}} \hat{a}_2^\dagger$, and (ii) the subsequent variable BS is defined by $\hat{B}_{23}(\theta) = e^{-\theta(\hat{a}_2^\dagger \hat{a}_3 - \hat{a}_2 \hat{a}_3^\dagger)}$, satisfying $\hat{B}_{23} \hat{a}_2^\dagger \hat{B}_{23}^\dagger = \sqrt{T} \hat{a}_2^\dagger - \sqrt{1-T} \hat{a}_3^\dagger$ and $\hat{B}_{23} \hat{a}_3^\dagger \hat{B}_{23}^\dagger = \sqrt{1-T} \hat{a}_2^\dagger + \sqrt{T} \hat{a}_3^\dagger$, where $T = \cos^2 \theta \in [0, 1]$. Notice that \hat{a}_j^\dagger (and \hat{a}_j) denotes the creation (and annihilation) operator of the j th mode. Consequently, the tritter can be represented by $\hat{T}_{123} = \hat{B}_{23}(\theta) \hat{B}_{12}(\pi/4)$. Therefore, we can generate a state yielding $|\psi\rangle_{123} = \hat{T}_{123} |\varepsilon\rangle_1 |0\rangle_2 |0\rangle_3$ by injecting $|\varepsilon\rangle$, $|0\rangle$, $|0\rangle$ into the corresponding input modes of the tritter. Upon straightforward derivation, the prepared state can be explicitly articulated as a three-qubit pure state

$$|\psi\rangle_{123} = c_0|000\rangle + c_1|100\rangle + c_2|010\rangle + c_3|001\rangle, \quad (1)$$

with $c_0 = \omega_0$, $c_1 = \omega_1/\sqrt{2}$, $c_2 = -\omega_1\sqrt{T/2}$, and $c_3 = \omega_1\sqrt{(1-T)/2}$. It is evident that the state $|\psi\rangle_{123}$ correlates with three interaction parameters (i.e., $|\alpha|$, ϕ , and T). This state exhibits a hybrid form of both GHZ-class and W -class states. Specifically, when $\alpha = 0$, $|\psi\rangle_{123}$ reduces to the simplest three-qubit product state $|000\rangle$. However, if $\alpha \neq 0$ and $T = 0$, $|\psi\rangle_{123}$ transforms into a biseparable state $(\omega_0|00\rangle + \frac{\omega_1}{\sqrt{2}}|10\rangle + \frac{\omega_1}{\sqrt{2}}|01\rangle)_{13} \otimes |0\rangle_2$. Similarly, if $\alpha \neq 0$ and $T = 1$, $|\psi\rangle_{123}$ becomes a biseparable state $(\omega_0|00\rangle + \frac{\omega_1}{\sqrt{2}}|10\rangle + \frac{\omega_1}{\sqrt{2}}|01\rangle)_{12} \otimes |0\rangle_3$.

III. TRIPARTITE ENTANGLEMENT

Concurrence is the most commonly used measure of entanglement. At the beginning, this measure was mainly used to study the entanglement for bipartite systems. In 2000, Coffman, Kundu, and Wootters first used the concurrence to study the entanglement distribution for the pure three-qubit states and showed the concurrence relation $C_{AB}^2 + C_{AC}^2 \leq C_{A(BC)}^2$ [19]. Later, this measure was also generalized to study ME, together with geometrical interpretation [50]. In this paper, we shall derive the $C_{i(jk)}$ -type concurrence (where i , j , and k are distinct values of 1, 2, or 3) and investigate the “genuine” tripartite entanglement of $|\psi\rangle_{123}$. Herein, $C_{i(jk)}$ represents the concurrence between a single party (inclusive of qubit i) and another party (encompassing qubits j and k).

A. $\mathcal{C}_{i(jk)}$ -type concurrence

Utilizing the Schmidt decomposition, we can derive the Schmidt coefficients ($\sqrt{\lambda_1}$ and $\sqrt{\lambda_2}$) for any bipartite pure state [51,52]. Consequently, the Schmidt weight can be ascertained through

$$Y = 1 - \sqrt{2(\lambda_1^2 + \lambda_2^2)} - 1. \quad (2)$$

The concurrence can be computed using

$$\mathcal{C}(Y) = \sqrt{Y(2 - Y)}. \quad (3)$$

When $|\psi\rangle_{123}$ is treated as a bipartite state, the corresponding Schmidt coefficients can be deduced (refer to Appendix A) and the $\mathcal{C}_{i(jk)}$ -type concurrence can be calculated according to Eqs. (2) and (3). The primary findings are presented as follows.

Case 1(23): In the bipartite scenario involving qubit 1 and pair 23, we observe that

$$Y_{1(23)} = 1 - \frac{\sqrt{2|\alpha|^2 + 1}}{|\alpha|^2 + 1}, \quad (4)$$

and

$$\mathcal{C}_{1(23)} = \frac{|\alpha|^2}{1 + |\alpha|^2} \equiv \Omega. \quad (5)$$

Case 2(31): In the bipartite scenario involving qubit 2 and pair 31, we observe that

$$Y_{2(31)} = 1 - \frac{\sqrt{(1 - T)^2|\alpha|^4 + 2|\alpha|^2 + 1}}{|\alpha|^2 + 1}, \quad (6)$$

and

$$\mathcal{C}_{2(31)} = \Omega\sqrt{T(2 - T)}. \quad (7)$$

Case 3(12): In the bipartite scenario involving qubit 3 and pair 12, we observe that

$$Y_{3(12)} = 1 - \frac{\sqrt{T^2|\alpha|^4 + 2|\alpha|^2 + 1}}{|\alpha|^2 + 1}, \quad (8)$$

and

$$\mathcal{C}_{3(12)} = \Omega\sqrt{1 - T^2}. \quad (9)$$

Clearly, all $\mathcal{C}_{i(jk)}$ s are contingent upon $|\alpha|$ and T , yet remain unaffected by ϕ . Subsequently, we will delve into the tripartite entanglement for $|\psi\rangle_{123}$, utilizing the measure associated with $\mathcal{C}_{i(jk)}$ -type concurrence.

B. Concurrence triangles and fill

In principle, any class of ME is linked to a geometric object, specifically an entanglement polytope [53]. Without a doubt, we can verify $\mathcal{C}_{i(jk)} \leq \mathcal{C}_{j(ki)} + \mathcal{C}_{k(ij)}$ for $|\psi\rangle_{123}$ as per Qian, Alonso, and Eberly [54]. Concurrently, we can also confirm

$$\mathcal{C}_{i(jk)}^2 \leq \mathcal{C}_{j(ki)}^2 + \mathcal{C}_{k(ij)}^2 \quad (10)$$

for $|\psi\rangle_{123}$, following the method of Zhu and Fei [33].

In accordance with Xie and Eberly [21], a concurrence triangle is constructed by defining $s_1 = \mathcal{C}_{1(23)}^2$, $s_2 = \mathcal{C}_{2(31)}^2$, and $s_3 = \mathcal{C}_{3(12)}^2$ as its three sides. It is well established that the

area of a triangle with side lengths (s_1, s_2, s_3) and perimeter $l = s_1 + s_2 + s_3$ can be computed using Heron's formula $\mathcal{A} = \frac{1}{4}[l(l - 2s_1)(l - 2s_2)(l - 2s_3)]^{1/2}$. For $|\psi\rangle_{123}$, we can obtain the triangle area

$$\mathcal{A}_{|\psi\rangle_{123}} = \Omega^4 T(1 - T)\sqrt{1 + T(1 - T)}, \quad (11)$$

and the concurrence fill [21,22]

$$F_{123} = F(|\psi\rangle_{123}) = \sqrt{\frac{4}{\sqrt{3}}\mathcal{A}_{|\psi\rangle_{123}}}. \quad (12)$$

That is, the concurrence fill is just the square root of the triangle area by multiplying $\sqrt{4/\sqrt{3}}$. Obviously, $\mathcal{A}_{|\psi\rangle_{123}}$ and F_{123} are dependent on $|\alpha|$ and T , but are independent of ϕ .

In Fig. 2, we give a table for the possible cases of $|\psi\rangle_{123}$, accompanying their corresponding conditions, concurrence triangles, areas, and fills. As highlighted by Dur *et al.* [12], all three-qubit states can be categorized into three distinct classes: product states, biseparable states, and nonbiseparable states. For $|\psi\rangle_{123}$, when $|\alpha| = 0$, the triangle is simplified to a single dot due to $s_1 = s_2 = s_3 = 0$, resulting in an area $\mathcal{A} = 0$ and $F_{123} = 0$. When $|\alpha| \neq 0$ and $T = 0$, the triangle is simplified to a line due to $s_1 = s_3 = \Omega^2 > 0$ and $s_2 = 0$, leading to an area $\mathcal{A} = 0$ and $F_{123} = 0$. When $|\alpha| \neq 0$ and $T = 1$, the triangle is simplified to a line due to $s_1 = s_2 = \Omega^2 > 0$ and $s_3 = 0$, resulting in an area $\mathcal{A} = 0$ and $F_{123} = 0$. Only when $|\alpha| \neq 0$ and $T \neq 0$ (or 1), does the triangle maintain its true form with appropriate $s_1, s_2, s_3 > 0$, accompanied by an area $\mathcal{A} > 0$ and $F_{123} > 0$.

As shown in Fig. 3, the value of $|\alpha|$ (or T) defines the shape (form) of the triangle for a fixed value of T (or $|\alpha|$). In each subfigure, one can see its respective values for three side lengths, the area, and the concurrence fill. Figures 3(a) to 3(c) depict the triangles with the same $|\alpha| = 5.5$ and different T (0.3, 0.5, and 0.7), accompanying different F_{123} (0.684394, 0.752832, and 0.684394). Figures 3(d) to 3(f) depict the triangles with same $T = 0.5$ and different $|\alpha|$ (1.5, 2.5, and 3.5), accompanying different F_{123} (0.3851, 0.5971, and 0.6867). In Fig. 4(a), we present the contour plot of F_{123} in the ($|\alpha|, T$) space. At the same time, we plot F_{123} as functions of $|\alpha|$ for several different T in Fig. 4(b) and F_{123} as functions of T for several different $|\alpha|$ in Fig. 4(c). Obviously, F_{123} is a symmetrical function of $T = 0.5$ and reaches its maximal values at $T = 0.5$ for each fixed $|\alpha|$. Meanwhile, F_{123} is a monotonically increasing function of $|\alpha|$ for each fixed T . At the limiting case of $|\psi\rangle_{123}$ with $|\alpha| \rightarrow \infty$ and $T = 0.5$, one can find a maximum value of F_{123} , i.e., 0.803428. As pointed out in Ref. [21], we also know $F_{123}(|\text{GHZ}\rangle) = 1$ and $F_{123}(|W\rangle) = 8/9 \doteq 0.889$. So, our considered state $|\psi\rangle_{123}$ is still less entangled than the GHZ state and the W state.

C. Checking GME

In the following, we shall check the five requirements for $F_{123}(|\psi\rangle_{123})$ one by one.

(R1) F_{123} is zero when $|\psi\rangle_{123}$ is a product state $|000\rangle$ for $|\alpha| = 0$ (see the fourth column in Fig. 2), or when $|\psi\rangle_{123}$ is a biseparate state for $|\alpha| \neq 0$, $T = 0$ (or $T = 1$) (see the second and third column in Fig. 2).

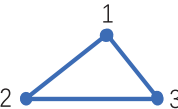



Conditions	$ \alpha \neq 0, T \neq 0$ (or 1)	$ \alpha \neq 0, T = 0$	$ \alpha \neq 0, T = 1$	$ \alpha = 0$
Triangles				
States	Nonbiseparable	Biseparable	Biseparable	Product
Areas	>0	$=0$	$=0$	$=0$
Concurrence Fill	>0	$=0$	$=0$	$=0$

FIG. 2. The table of possible cases of $|\psi\rangle_{123}$ and their corresponding conditions, concurrence triangles, areas, and fills.

(R2) F_{123} is positive if $|\psi\rangle_{123}$ is a nonbiseparate state for $|\alpha| \neq 0, T \neq 0$ (or $T \neq 1$) (see the first column in Fig. 2).

(R3) As pointed out by Xie and Eberly [21], concurrence fill can be constructed as the convex roof, i.e., $F_{123}(\rho) = \min_{\{p_i, |\psi_i\rangle\}} \sum_i p_i F_{123}(|\psi_i\rangle)$, over all possible decomposition $\rho = \sum_i p_i |\psi_i\rangle\langle\psi_i|$. So, it is satisfying the convex relation

with $F_{123}(\sum_i p_i |\psi_i\rangle\langle\psi_i|) \leq \sum_i p_i F_{123}(|\psi_i\rangle\langle\psi_i|)$. Obviously, this requirement is true for $|\psi\rangle_{123}$ by taking the equal sign.

(R4) Following the arguments in Refs. [12,22,23] and through numerical search in all parameter space, we find that $F_{123}(|\psi\rangle_{123})$ is nonincreasing under LOCC, i.e., $F_{123}[\Lambda_{\text{LOCC}}(|\psi\rangle_{123})] \leq F_{123}(|\psi\rangle_{123})$. The details on the LOCC monotonicity are provided in Appendix B.

(R5) Since $C_{i(jk)}$ can be also obtained in another way through $\sqrt{2[1 - \text{Tr}(\rho_i^2)]}$ [$\rho_i = \text{Tr}_{jk}(\rho_{123})$], it is clear that $F_{123}(|\psi\rangle_{123})$ is invariant under local unitary operations.

Then, we say, $F_{123}(|\psi\rangle_{123})$ is a proper genuine tripartite entanglement measure.

IV. TRIPARTITE STEERING

Inspired by the work of Hao *et al.* [37], we shall analyze the tripartite EPR steering in $|\psi\rangle_{123}$ by using the uncertainty relations [55] under specific measurement settings.

A. Theoretical proposal and relation

We assume that qubits 1, 2, and 3 are controlled by Alice, Bob, and Charlie, respectively, with three measurement settings $\{\sigma_x, \sigma_y, \sigma_z\}$. In detail, we define these observables as $A_1 = \sigma_x^{(1)}, A_2 = \sigma_y^{(1)}, A_3 = \sigma_z^{(1)}$; $B_1 = \sigma_x^{(2)}, B_2 = \sigma_y^{(2)}, B_3 = \sigma_z^{(2)}$; $C_1 = \sigma_x^{(3)}, C_2 = \sigma_y^{(3)}, C_3 = \sigma_z^{(3)}$, where

$$\sigma_x^{(k)} = \begin{pmatrix} 0 & 1 \\ 1 & 0 \end{pmatrix}, \quad \sigma_y^{(k)} = \begin{pmatrix} 0 & -i \\ i & 0 \end{pmatrix}, \quad \sigma_z^{(k)} = \begin{pmatrix} 1 & 0 \\ 0 & -1 \end{pmatrix}, \quad (13)$$

denote the standard Pauli spin operators for the k th qubit.

In the subsequent sections, we define the uncertainty of an observable X on a state ρ as the variance $\delta^2 X = \langle X^2 \rangle - \langle X \rangle^2$. Here, $\langle X \rangle$ represents the expectation value of X , calculated as $\langle X \rangle = \text{Tr}(X\rho)$. Furthermore, $C(X, Y) = \langle XY \rangle - \langle X \rangle \langle Y \rangle$ denotes the covariance between observable X and observable Y . To ascertain the configuration of EPR steering, we may employ the following criterion based on uncertainty relations.

(1) *Alice can steer Bob* if the inequality

$$P_{AB} = \sum_i \delta^2(\alpha_i^{(AB)} A_i + B_i) \geq \min_{\rho_B} \sum_i \delta^2 B_i \quad (14)$$

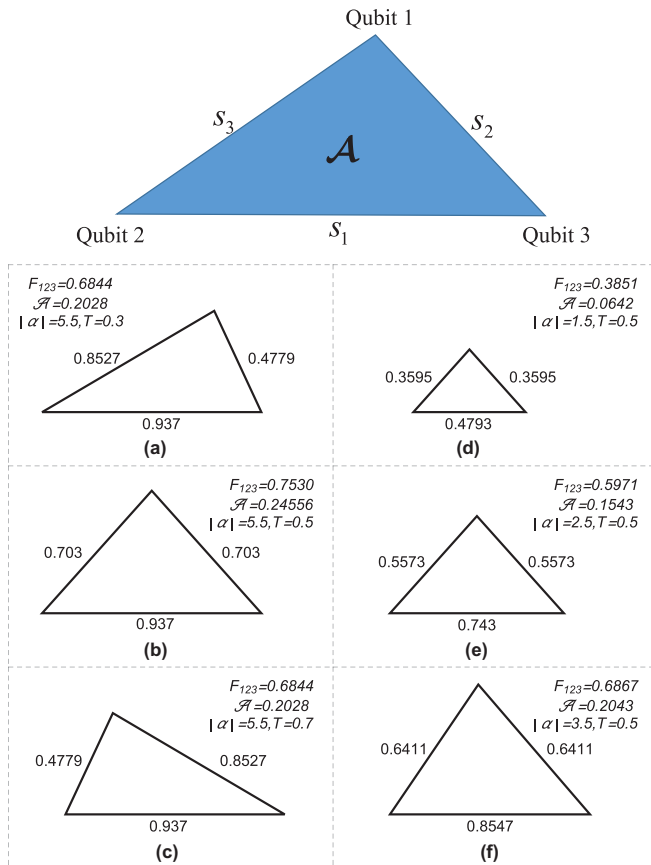


FIG. 3. Top: The concurrence triangle for a three-qubit state $|\psi\rangle_{123}$, with its three side lengths $s_1 = C_{1(23)}^2$, $s_2 = C_{2(31)}^2$, and $s_3 = C_{3(12)}^2$. Bottom: Six triangles are depicted by taking $(|\alpha|, T)$ values with (a) (5.5, 0.3), (b) (5.5, 0.5), (c) (5.5, 0.7), (d) (1.5, 0.5), (e) (2.5, 0.5), and (f) (3.5, 0.5), respectively. The corresponding areas and concurrence fills are also provided.

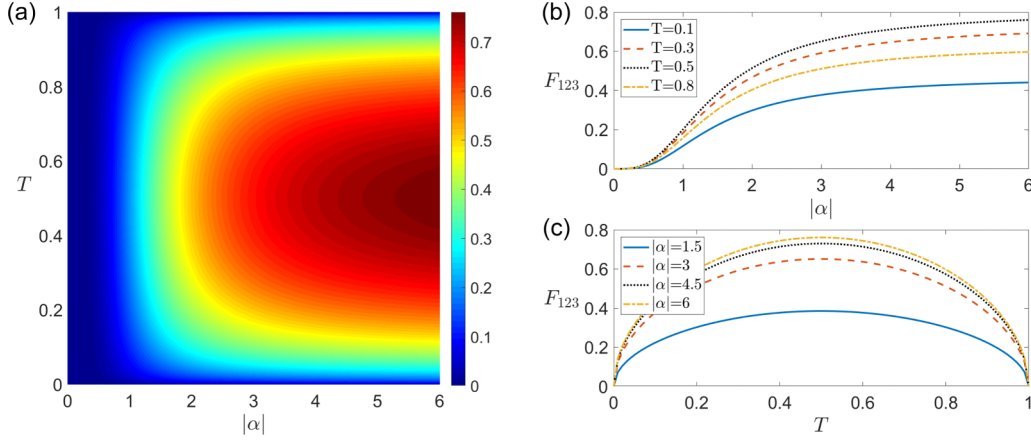


FIG. 4. (a) Contour plot of the concurrence fill $F_{123}(|\psi\rangle_{123})$ in the $(|\alpha|, T)$ space; (b) F_{123} versus $|\alpha|$ with $T = 0.1, 0.3, 0.5, 0.8$; (c) F_{123} versus T with $|\alpha| = 1.5, 3, 4.5, 6$.

is violated, where

$$\alpha_i^{(AB)} = \begin{cases} -\frac{C(A_i, B_i)}{\delta^2 A_i}, & \text{if } \delta^2 A_i \neq 0; \\ -\frac{\delta^2 B_i}{2C(A_i, B_i)}, & \text{if } \delta^2 A_i = 0, C(A_i, B_i) \neq 0; \\ 0, & \text{if } \delta^2 A_i = 0, C(A_i, B_i) = 0. \end{cases} \quad (15)$$

(2) *Bob can steer Alice* if the inequality

$$P_{BA} = \sum_i \delta^2 (\beta_i^{(BA)} B_i + A_i) \geq \min_{\rho_A} \sum_i \delta^2 A_i \quad (16)$$

is violated, where

$$\beta_i^{(BA)} = \begin{cases} -\frac{C(A_i, B_i)}{\delta^2 B_i}, & \text{if } \delta^2 B_i \neq 0; \\ -\frac{\delta^2 A_i}{2C(A_i, B_i)}, & \text{if } \delta^2 B_i = 0, C(A_i, B_i) \neq 0; \\ 0, & \text{if } \delta^2 B_i = 0, C(A_i, B_i) = 0. \end{cases} \quad (17)$$

(3) *Alice can steer Charlie* if the inequality

$$P_{AC} = \sum_i \delta^2 (\alpha_i^{(AC)} A_i + C_i) \geq \min_{\rho_C} \sum_i \delta^2 C_i \quad (18)$$

is violated, where

$$\alpha_i^{(AC)} = \begin{cases} -\frac{C(A_i, C_i)}{\delta^2 A_i}, & \text{if } \delta^2 A_i \neq 0; \\ -\frac{\delta^2 C_i}{2C(A_i, C_i)}, & \text{if } \delta^2 A_i = 0, C(A_i, C_i) \neq 0; \\ 0, & \text{if } \delta^2 A_i = 0, C(A_i, C_i) = 0. \end{cases}$$

(4) *Charlie can steer Alice* if the inequality

$$P_{CA} = \sum_i \delta^2 (\gamma_i^{(CA)} C_i + A_i) \geq \min_{\rho_A} \sum_i \delta^2 A_i \quad (19)$$

is violated, where

$$\gamma_i^{(CA)} = \begin{cases} -\frac{C(A_i, C_i)}{\delta^2 C_i}, & \text{if } \delta^2 C_i \neq 0; \\ -\frac{\delta^2 A_i}{2C(A_i, C_i)}, & \text{if } \delta^2 C_i = 0, C(A_i, C_i) \neq 0; \\ 0, & \text{if } \delta^2 C_i = 0, C(A_i, C_i) = 0. \end{cases} \quad (20)$$

(5) *Bob can steer Charlie* if the inequality

$$P_{BC} = \sum_i \delta^2 (\beta_i^{(BC)} B_i + C_i) \geq \min_{\rho_C} \sum_i \delta^2 C_i \quad (21)$$

is violated, where

$$\beta_i^{(BC)} = \begin{cases} -\frac{C(B_i, C_i)}{\delta^2 B_i}, & \text{if } \delta^2 B_i \neq 0; \\ -\frac{\delta^2 C_i}{2C(B_i, C_i)}, & \text{if } \delta^2 B_i = 0, C(B_i, C_i) \neq 0; \\ 0, & \text{if } \delta^2 B_i = 0, C(B_i, C_i) = 0. \end{cases} \quad (22)$$

(6) *Charlie can steer Bob* if the inequality

$$P_{CB} = \sum_i \delta^2 (\gamma_i^{(CB)} C_i + B_i) \geq \min_{\rho_B} \sum_i \delta^2 B_i \quad (23)$$

is violated, where

$$\gamma_i^{(CB)} = \begin{cases} -\frac{C(B_i, C_i)}{\delta^2 C_i}, & \text{if } \delta^2 C_i \neq 0; \\ -\frac{\delta^2 B_i}{2C(B_i, C_i)}, & \text{if } \delta^2 C_i = 0, C(B_i, C_i) \neq 0; \\ 0, & \text{if } \delta^2 C_i = 0, C(B_i, C_i) = 0. \end{cases} \quad (24)$$

Some analytical results for calculating P_{AB} , P_{BA} , P_{AC} , P_{CA} , P_{BC} , and P_{CB} are listed in Appendix C. For our used setting, we can get $\min_{\rho_A} \sum_i \delta^2 A_i = 2$, $\min_{\rho_B} \sum_i \delta^2 B_i = 2$, and $\min_{\rho_C} \sum_i \delta^2 C_i = 2$. Physically, if $P_{ij} < 2$, then we say that party- i can steer party- j . In particular, we have $P_{AB} = P_{BA} = P_{AC} = P_{CA} = P_{BC} = P_{CB} = 2$ in the limiting case of $|\alpha| = 0$, corresponding to product state $|000\rangle$.

B. Numerical simulation and analysis

Using the above analytical expressions from Eqs. (14) to (24), we make numerical simulation for the tripartite steering of $|\psi\rangle_{123}$.

In Fig. 5, we plot the feasible regions satisfying $P_{AB} < 2$, $P_{BA} < 2$, $P_{AC} < 2$, and $P_{CA} < 2$, in $(|\alpha|, \phi, T)$ parameter space by setting $0 \leq T \leq 1$, $0 \leq |\alpha| \leq 6$, and $0 \leq \phi \leq \pi$. Note that all P_{ij} s are periodic functions of ϕ with period $\pi/2$. Moreover, it is symmetric with respect to $\phi = \pi/4$ in the range $\phi \in (0, \pi/2)$. However, no matter what parameter $(|\alpha|, \phi, T)$ values we choose, it is impossible to satisfy $P_{BC} < 2$ and $P_{CB} < 2$. That is to say, regions with $P_{BC} < 2$ and $P_{CB} < 2$ are empty, which means that there is no steering between B and C .

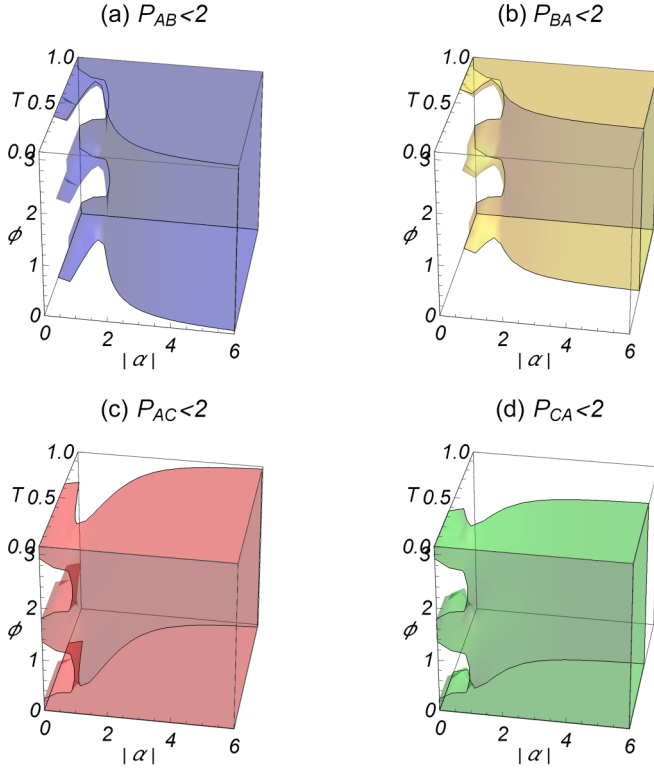


FIG. 5. The feasibility regions satisfying (a) $P_{AB} < 2$, (b) $P_{BA} < 2$, (c) $P_{AC} < 2$, (d) $P_{CA} < 2$, in the parameters $(|\alpha|, \phi, T)$ space with $|\alpha| \in [0, 6]$, $\phi \in [0, \pi]$, $T \in [0, 1]$.

Undoubtedly, each subfigure in Fig. 5 only shows its respective one-way steerability. The common region in Figs. 5(a) and 5(b), satisfying $P_{AB} < 2$ and $P_{BA} < 2$ simultaneously, will exhibit two-way steering between A and B. Similarly, the common region in Figs. 5(c) and 5(d), satisfying $P_{AC} < 2$ and $P_{CA} < 2$ simultaneously, will exhibit two-way steering between A and C. Moreover, the regions with no steering are different for these subfigures.

In Fig. 6, we depict three $(|\alpha|, T)$ planes by maintaining $\phi = 0, 0.1\pi, 0.25\pi$ and illustrate nine distinct configurations of steerability relations for $|\psi\rangle_{123}$. Meanwhile, these configurations are detailed in Table I and further elucidated in Fig. 7. The implication of each configuration (here abbreviated as Cf.) can be explained as follows.

Cf. “a” signifies that Alice, Bob, and Charlie are unable to steer each other (no steering).

Cf. “b” denotes that only Alice and Bob can steer each other (two-way steering).

Cf. “c” indicates that solely Alice can steer Bob (one-way steering). In this configuration, Bob cannot be steered by Alice and Charlie simultaneously (a monogamy).

Cf. “d” represents that: (1) Alice and Bob can steer each other (two-way steering), and 2) Alice can steer Charlie (one-way steering).

Cf. “e” signifies that: (1) Alice and Bob can steer each other (two-way steering), and (2) Alice and Charlie can steer each other (two-way steering). In this configuration, Bob and Charlie can simultaneously steer Alice (a shareability).

Cf. “f” suggests that: (1) Alice can steer Bob (one-way steering), and (2) Alice can steer Charlie (one-way steering).

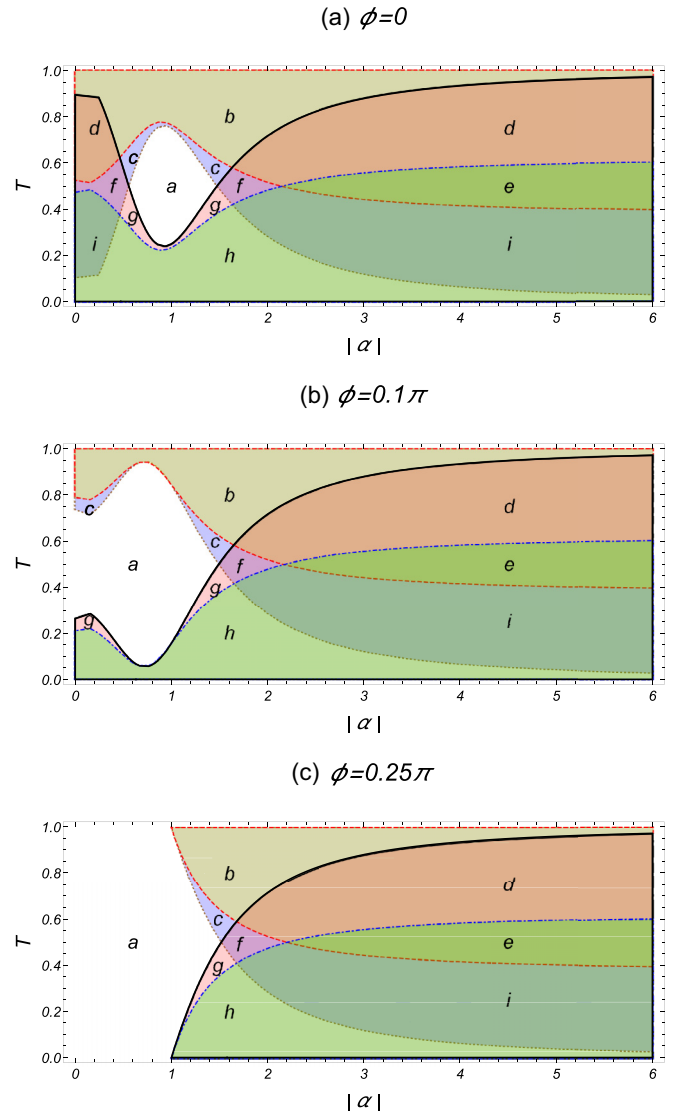


FIG. 6. Three $(|\alpha|, T)$ planes illustrate nine distinct configurations of steerability for $|\psi\rangle_{123}$, characterized by (a) $\phi = 0$, (b) $\phi = 0.1\pi$, (c) $\phi = 0.25\pi$, respectively. The regions delineated by the colors correspond to these varying configurations.

Cf. “g” implies that only Alice can steer Charlie (one-way steering). In this configuration, Charlie cannot be steered by Alice and Bob simultaneously (a monogamy).

TABLE I. Nine configurations (in Figs. 6, 7) and their respective steerings.

Configurations	P_{AB}	P_{BA}	P_{AC}	P_{CA}	P_{BC}	P_{CB}
(a)	≥ 2	≥ 2	≥ 2	≥ 2	≥ 2	≥ 2
(b)	< 2	< 2	≥ 2	≥ 2	≥ 2	≥ 2
(c)	< 2	≥ 2	≥ 2	≥ 2	≥ 2	≥ 2
(d)	< 2	< 2	< 2	≥ 2	≥ 2	≥ 2
(e)	< 2	< 2	< 2	< 2	≥ 2	≥ 2
(f)	< 2	≥ 2	< 2	≥ 2	≥ 2	≥ 2
(g)	≥ 2	≥ 2	< 2	≥ 2	≥ 2	≥ 2
(h)	≥ 2	≥ 2	< 2	< 2	≥ 2	≥ 2
(i)	< 2	≥ 2	< 2	< 2	≥ 2	≥ 2

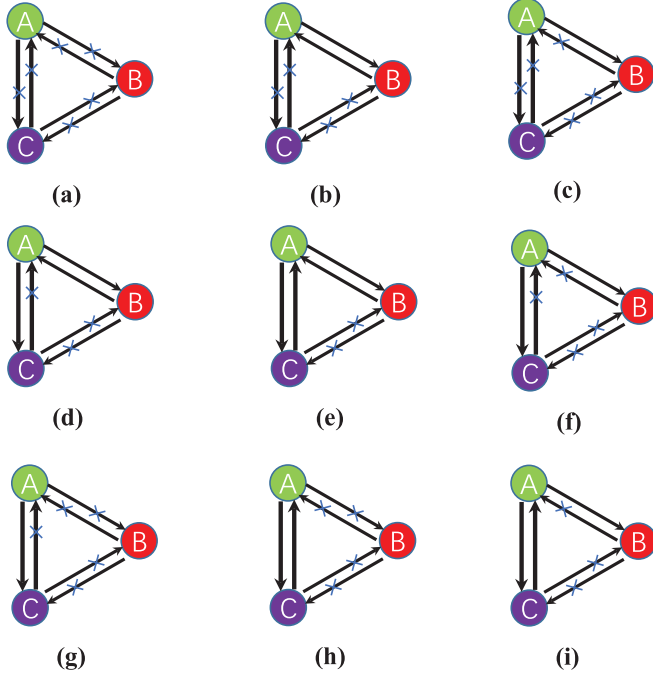


FIG. 7. The configurations of tripartite steerings, which are shared among three observers (A, B, and C), correspond to regions delineated from (a) to (i) in Fig. 6.

Cf. “h” indicates that only Alice and Charlie can steer each other (two-way steering).

Cf. “i” signifies that: (1) Alice and Charlie can steer each other (two-way steering), and 2) Alice can steer Bob (one-way steering).

Our configurations, further illustrated in Fig. 7 and Table I, can reflect their respective steering relations. For example, when $\phi = 0.1\pi$, $|\alpha| = 3.5$, and $T = 0.5$, we have $P_{AB} = 1.6719(4)$, $P_{BA} = 1.8397(6)$, $P_{AC} = 1.6719(4)$, $P_{CA} = 1.8397(6)$, $P_{BC} = 2.1978(1)$, and $P_{CB} = 2.1978(1)$. This case corresponds to Fig. 7(e).

As examples, we depict all P_{ij} s as functions of one parameter by fixing other two parameters of $|\psi\rangle_{123}$ in Fig. 8. Through solving $P_{ij} = 2$, we can obtain the intersection points in each subfigure and divide different ranges. For each range, we can identify its corresponding configuration. Figure 8(a) presents all P_{ij} s versus $|\alpha| \in [0, 6]$ for $\phi = 0.1\pi$ and $T = 0.3$, where the ranges of $|\alpha| \in (0, 1.19751)$, $(1.19751, 1.28267)$, $(1.28267, 1.94563)$, and $(1.94563, \infty)$ correspond to configurations of Figs. 8(a), 8(g), 8(h), and 8(i). Figure 8(b) presents all P_{ij} s versus $\phi \in [0, \pi]$ for $|\alpha| = 0.2$ and $T = 0.3$, where the ranges of $\phi \in (0, 0.175126)$, $(0.175126, 0.266456)$, $(0.266456, 0.306136)$, and $(0.306136, \pi/4)$ correspond to configurations of Figs. 8(i), 8(h), 8(g), and 8(a). Here, we only analyze the variations in the range $\phi \in [0, \pi/4]$ because all P_{ij} s are the periodic functions with period $\pi/2$ and symmetrical in each period. Figure 8(c) presents all P_{ij} s versus $T \in [0, 1]$ for $\phi = 0.1\pi$ and $|\alpha| = 0.2$, where the ranges of $T \in (0, 0.210711)$, $(0.210711, 0.271447)$, $(0.271447, 0.728553)$, $(0.728553, 0.789289)$, and $(0.789289, 1)$ correspond to configurations of Figs. 8(h), 8(g), 8(a), 8(c), and 8(b).

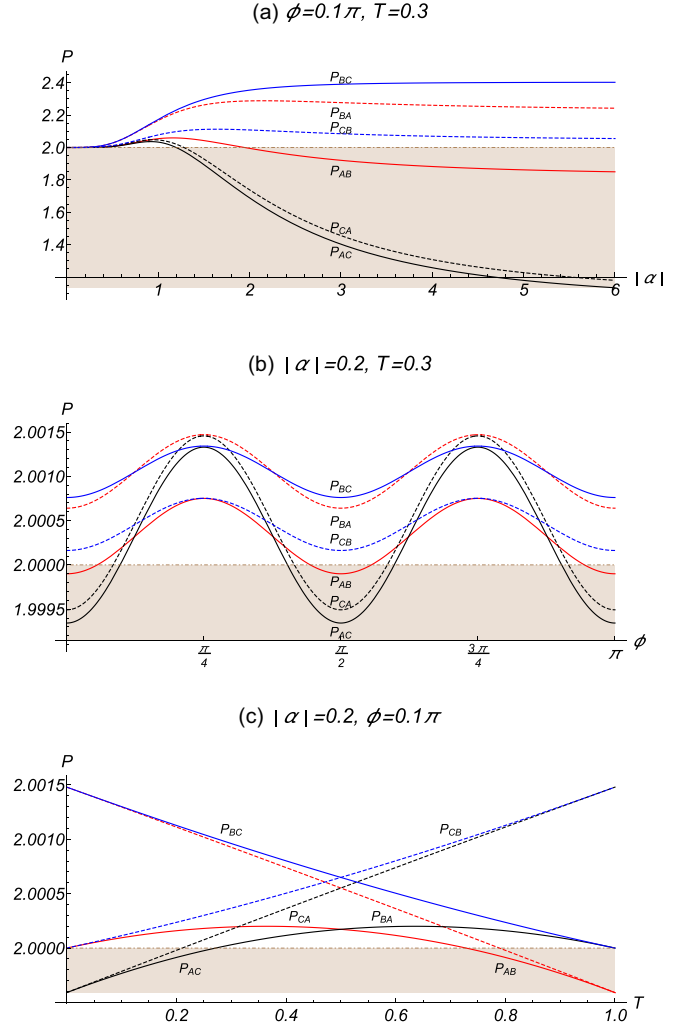


FIG. 8. (a) P versus $|\alpha|$ with fixed $\phi = 0.1\pi$ and $T = 0.3$; (b) P versus ϕ with fixed $|\alpha| = 0.2$ and $T = 0.3$; (c) P versus T with fixed $|\alpha| = 0.2$ and $\phi = 0.1\pi$.

V. SUMMARY AND CONCLUSION

In this study, we introduced a scheme for preparing a specific class of three-qubit states and conducted a theoretical exploration of tripartite entanglement and steering. These prepared states exhibit a hybrid form, combining GHZ-like and W-like characteristics of three-qubit states. Through the construction of a concurrence triangle, we demonstrated that our three-qubit state possesses genuine tripartite entanglement. Utilizing certain measurements and applying the uncertainty relations criterion, we identified nine distinct configurations of tripartite steering. Notably, most of these configurations adhere to shareability without being constrained by monogamy. Throughout the paper, we provided comprehensive analytical expressions and numerical results based on selected interaction parameters. Upon thorough comparison and analysis, it was determined that while the state exhibits entanglement, steering was unattainable in a significant portion of the parameter space.

Our scheme has the advantages of using linear optics to prepare three-qubit quantum states. With the help of BSs and

photon-number-resolved detections, we think, these states can be easily realized in experiments, especially by virtue of the QS technique [56–58]. Currently, there are many methods to experimentally detect quantum correlations (including entanglement and steering) [59–62]. Moreover, some measurements (especially on qubits) are relatively mature in the field of quantum information science [63,64]. With current technology, we also think that detection for our studied tripartite entanglement and steering can be implemented in experiments.

ACKNOWLEDGMENTS

This paper was supported by the National Natural Science Foundation of China (Grants No. 12465004 and No. 11665013). We thank Bi-xuan Fan and Hong-chun Yuan for the useful discussion.

APPENDIX A: SCHMIDT COEFFICIENTS FOR CALCULATING

$C_{i(jk)}$ -type concurrence

In accordance with the bipartite cases of $|\psi\rangle_{123}$, we present the following Schmidt coefficients (λ_1 s and λ_2 s) through the implementation of a Schmidt decomposition [52].

(1) *Case 1(23)*: If $|\psi\rangle_{123}$ is reexpressed as

$$|\psi\rangle_{123} = (|0\rangle_1 \quad |1\rangle_1)M_1 \begin{pmatrix} |00\rangle_{23} \\ |10\rangle_{23} \\ |01\rangle_{23} \\ |11\rangle_{23} \end{pmatrix}, \quad (\text{A1})$$

with $M_1 = \begin{pmatrix} c_0 & c_2 & c_3 & 0 \\ c_1 & 0 & 0 & 0 \end{pmatrix}$, then $|\psi\rangle_{123}$ can be further decomposed into the Schmidt form like Eq. (17) in Ref. [54] with the Schmidt coefficients $\sqrt{\lambda_1^{(1)}}$ and $\sqrt{\lambda_2^{(1)}}$, where

$$\begin{aligned} \lambda_1^{(1)} &= \frac{1}{2} + \frac{\sqrt{2|\alpha|^2 + 1}}{2(|\alpha|^2 + 1)}, \\ \lambda_2^{(1)} &= \frac{1}{2} - \frac{\sqrt{2|\alpha|^2 + 1}}{2(|\alpha|^2 + 1)}, \end{aligned} \quad (\text{A2})$$

are the eigenvalues of $M_1 M_1^\dagger$.

(2) *Case 2(13)*: If $|\psi\rangle_{123}$ is reexpressed as

$$|\psi\rangle_{123} = (|0\rangle_2 \quad |1\rangle_2)M_2 \begin{pmatrix} |00\rangle_{13} \\ |10\rangle_{13} \\ |01\rangle_{13} \\ |11\rangle_{13} \end{pmatrix}, \quad (\text{A3})$$

with $M_2 = \begin{pmatrix} c_0 & c_1 & c_3 & 0 \\ c_2 & 0 & 0 & 0 \end{pmatrix}$, then $|\psi\rangle_{123}$ can be further decomposed into the Schmidt form like Eq. (17) in Ref. [54] with the Schmidt coefficients $\sqrt{\lambda_1^{(2)}}$ and $\sqrt{\lambda_2^{(2)}}$, where

$$\begin{aligned} \lambda_1^{(2)} &= \frac{1}{2} + \frac{\sqrt{(1-T)^2|\alpha|^4 + 2|\alpha|^2 + 1}}{2(|\alpha|^2 + 1)}, \\ \lambda_2^{(2)} &= \frac{1}{2} - \frac{\sqrt{(1-T)^2|\alpha|^4 + 2|\alpha|^2 + 1}}{2(|\alpha|^2 + 1)}, \end{aligned} \quad (\text{A4})$$

are the eigenvalues of $M_2 M_2^\dagger$.

(3) *Case 3(12)*: If $|\psi\rangle_{123}$ is reexpressed as

$$|\psi\rangle_{123} = (|0\rangle_3 \quad |1\rangle_3)M_3 \begin{pmatrix} |00\rangle_{12} \\ |10\rangle_{12} \\ |01\rangle_{12} \\ |11\rangle_{12} \end{pmatrix}, \quad (\text{A5})$$

with $M_3 = \begin{pmatrix} c_0 & c_1 & c_2 & 0 \\ c_3 & 0 & 0 & 0 \end{pmatrix}$, then $|\psi\rangle_{123}$ can be further decomposed into the Schmidt form like Eq. (17) in Ref. [54] with the Schmidt coefficients $\sqrt{\lambda_1^{(3)}}$ and $\sqrt{\lambda_2^{(3)}}$, where

$$\begin{aligned} \lambda_1^{(3)} &= \frac{1}{2} + \frac{\sqrt{T^2|\alpha|^4 + 2|\alpha|^2 + 1}}{2(|\alpha|^2 + 1)}, \\ \lambda_2^{(3)} &= \frac{1}{2} - \frac{\sqrt{T^2|\alpha|^4 + 2|\alpha|^2 + 1}}{2(|\alpha|^2 + 1)}, \end{aligned} \quad (\text{A6})$$

are the eigenvalues of $M_3 M_3^\dagger$.

APPENDIX B: CHECKING LOCC MONOTONICITY OF CONCURRENCE FILL

Following the methods in Refs. [12,22,23], we check the LOCC monotonicity of $F_{123}(|\psi\rangle_{123})$.

First, we set $X_1 = D_1 V$ and $X_2 = D_2 V$ as binary-outcome positive-operator-valued measures (POVMs) satisfying $X_1^\dagger X_1 + X_2^\dagger X_2 = \hat{I}$ (\hat{I} is a 2×2 identity matrix), where

$$D_1 = \begin{pmatrix} \sin \theta_1 & 0 \\ 0 & \sin \theta_2 \end{pmatrix}, \quad D_2 = \begin{pmatrix} \cos \theta_1 & 0 \\ 0 & \cos \theta_2 \end{pmatrix}, \quad (\text{B1})$$

and

$$V = \begin{pmatrix} \cos \varkappa_1 & -e^{i\varkappa_2} \sin \varkappa_1 \\ \sin \varkappa_1 & e^{i\varkappa_2} \cos \varkappa_1 \end{pmatrix}, \quad (\text{B2})$$

with $\theta_i, \varkappa_i \in [-\pi, \pi]$.

Second, acting X_1 and X_2 on the mode-1 of $|\psi\rangle_{123}$, we obtain

$$|\psi^{(1)}\rangle_{123} = \frac{1}{\sqrt{p_1}}(X_1 \otimes \hat{I} \otimes \hat{I})|\psi\rangle_{123}, \quad (\text{B3})$$

and

$$|\psi^{(2)}\rangle_{123} = \frac{1}{\sqrt{p_2}}(X_2 \otimes \hat{I} \otimes \hat{I})|\psi\rangle_{123}, \quad (\text{B4})$$

respectively. Here p_1 and p_2 denote their respective success probability, satisfying $p_1 + p_2 = 1$.

Third, we calculate $F(|\psi^{(1)}\rangle_{123})$ and $F(|\psi^{(2)}\rangle_{123})$ and check LOCC monotonicity. Through numerical search, we find that the following inequality:

$$F(|\psi\rangle_{123}) - \sum_{i=1}^2 p_i F(|\psi^{(i)}\rangle_{123}) \geq 0 \quad (\text{B5})$$

is always satisfied in all possible parameters (including $|\alpha|$, ϕ , T , θ_1 , θ_2 , \varkappa_1 , and \varkappa_2) space. Since it is nonincreasing under the LOCC, we say that the concurrence fill is entanglement monotone at least for our considered state $|\psi\rangle_{123}$ and under our chosen POVMs.

Moreover, similar conclusions can be obtained when the LOCC operations are employed on mode-2 and mode-3.

APPENDIX C: ANALYTICAL EXPRESSIONS OF VARIANCES AND COVARIANCES

Within the defined space spanned by $\{|000\rangle, |001\rangle, |010\rangle, |011\rangle, |100\rangle, |101\rangle, |110\rangle, |111\rangle\}$, the density operator $\rho_{123} = |\psi\rangle_{123}\langle\psi|$ can be comprehensively expanded into a matrix representation

$$\rho_{123} = \begin{pmatrix} \frac{1}{|\alpha|^2+1} & \frac{\alpha\sqrt{2(1-T)}}{2(|\alpha|^2+1)} & -\frac{\alpha\sqrt{2T}}{2(|\alpha|^2+1)} & 0 & \frac{\alpha\sqrt{2}}{2(|\alpha|^2+1)} & 0 & 0 & 0 \\ \frac{\alpha^*\sqrt{2(1-T)}}{2(|\alpha|^2+1)} & \frac{|\alpha|^2(1-T)}{2(|\alpha|^2+1)} & -\frac{|\alpha|^2\sqrt{T(1-T)}}{2(|\alpha|^2+1)} & 0 & \frac{|\alpha|^2\sqrt{1-T}}{2(|\alpha|^2+1)} & 0 & 0 & 0 \\ -\frac{\alpha^*\sqrt{2T}}{2(|\alpha|^2+1)} & -\frac{|\alpha|^2\sqrt{T(1-T)}}{2(|\alpha|^2+1)} & \frac{|\alpha|^2T}{2(|\alpha|^2+1)} & 0 & -\frac{|\alpha|^2\sqrt{T}}{2(|\alpha|^2+1)} & 0 & 0 & 0 \\ 0 & 0 & 0 & 0 & 0 & 0 & 0 & 0 \\ \frac{\alpha^*\sqrt{2}}{2(|\alpha|^2+1)} & \frac{|\alpha|^2\sqrt{1-T}}{2(|\alpha|^2+1)} & -\frac{|\alpha|^2\sqrt{T}}{2(|\alpha|^2+1)} & 0 & \frac{|\alpha|^2}{2(|\alpha|^2+1)} & 0 & 0 & 0 \\ 0 & 0 & 0 & 0 & 0 & 0 & 0 & 0 \\ 0 & 0 & 0 & 0 & 0 & 0 & 0 & 0 \\ 0 & 0 & 0 & 0 & 0 & 0 & 0 & 0 \end{pmatrix}.$$

The following variances and covariances can be provided for the selected observables.

(1) Three variances for Alice are

$$\begin{aligned} \delta^2 A_1 &= \frac{|\alpha|^4 + (1 - \cos 2\phi)|\alpha|^2 + 1}{(|\alpha|^2 + 1)^2}, \\ \delta^2 A_2 &= \frac{|\alpha|^4 + (1 + \cos 2\phi)|\alpha|^2 + 1}{(|\alpha|^2 + 1)^2}, \\ \delta^2 A_3 &= \frac{|\alpha|^4 + 2|\alpha|^2}{(|\alpha|^2 + 1)^2}, \end{aligned} \quad (C1)$$

which lead to

$$\sum_i \delta^2 A_i = \frac{3|\alpha|^4 + 4|\alpha|^2 + 2}{(|\alpha|^2 + 1)^2}. \quad (C2)$$

(2) Three variances for Bob are

$$\begin{aligned} \delta^2 B_1 &= \frac{|\alpha|^4 + (2 - T - T \cos 2\phi)|\alpha|^2 + 1}{(|\alpha|^2 + 1)^2}, \\ \delta^2 B_2 &= \frac{|\alpha|^4 + (2 - T + T \cos 2\phi)|\alpha|^2 + 1}{(|\alpha|^2 + 1)^2}, \\ \delta^2 B_3 &= \frac{(2T - T^2)|\alpha|^4 + 2T|\alpha|^2}{(|\alpha|^2 + 1)^2}, \end{aligned} \quad (C3)$$

which lead to

$$\sum_i \delta^2 B_i = \frac{(2 + 2T - T^2)|\alpha|^4 + 4|\alpha|^2 + 2}{(|\alpha|^2 + 1)^2}. \quad (C4)$$

(3) Three variances for Charlie are

$$\begin{aligned} \delta^2 C_1 &= \frac{|\alpha|^4 + (1 + T - (1 - T) \cos 2\phi)|\alpha|^2 + 1}{(|\alpha|^2 + 1)^2}, \\ \delta^2 C_2 &= \frac{|\alpha|^4 + (1 + T + (1 - T) \cos 2\phi)|\alpha|^2 + 1}{(|\alpha|^2 + 1)^2}, \\ \delta^2 C_3 &= \frac{(1 - T^2)|\alpha|^4 + 2(1 - T)|\alpha|^2}{(|\alpha|^2 + 1)^2}, \end{aligned} \quad (C5)$$

which lead to

$$\sum_i \delta^2 C_i = \frac{(3 - T^2)|\alpha|^4 + 4|\alpha|^2 + 2}{(|\alpha|^2 + 1)^2}. \quad (C6)$$

(4) Three covariances between Alice and Bob are

$$\begin{aligned} C(A_1, B_1) &= -\frac{\sqrt{T}(|\alpha|^4 - |\alpha|^2 \cos 2\phi)}{(|\alpha|^2 + 1)^2}, \\ C(A_2, B_2) &= -\frac{\sqrt{T}(|\alpha|^4 + |\alpha|^2 \cos 2\phi)}{(|\alpha|^2 + 1)^2}, \\ C(A_3, B_3) &= -\frac{T|\alpha|^4}{(|\alpha|^2 + 1)^2}. \end{aligned} \quad (C7)$$

(5) Three covariances between Alice and Charlie are

$$\begin{aligned} C(A_1, C_1) &= \frac{\sqrt{1-T}(|\alpha|^4 - |\alpha|^2 \cos 2\phi)}{(|\alpha|^2 + 1)^2}, \\ C(A_2, C_2) &= \frac{\sqrt{1-T}(|\alpha|^4 + |\alpha|^2 \cos 2\phi)}{(|\alpha|^2 + 1)^2}, \\ C(A_3, C_3) &= -\frac{(1-T)|\alpha|^4}{(|\alpha|^2 + 1)^2}. \end{aligned} \quad (C8)$$

(6) Three covariances between Bob and Charlie are

$$\begin{aligned} C(B_1, C_1) &= -\frac{\sqrt{T(1-T)}(|\alpha|^4 - |\alpha|^2 \cos 2\phi)}{(|\alpha|^2 + 1)^2}, \\ C(B_2, C_2) &= -\frac{\sqrt{T(1-T)}(|\alpha|^4 + |\alpha|^2 \cos 2\phi)}{(|\alpha|^2 + 1)^2}, \\ C(B_3, C_3) &= -\frac{T(1-T)|\alpha|^4}{(|\alpha|^2 + 1)^2}. \end{aligned} \quad (C9)$$

- [1] R. Horodecki, P. Horodecki, M. Horodecki, and K. Horodecki, Quantum entanglement, *Rev. Mod. Phys.* **81**, 865 (2009).
- [2] O. Gühne and G. Toth, Entanglement detection, *Phys. Rep.* **474**, 1 (2009).
- [3] M. A. Nielsen and I. L. Chuang, *Quantum Computation and Quantum Information* (Cambridge University Press, Cambridge, England, 2000).
- [4] N. Linden and S. Popescu, Good dynamics versus bad kinematics: Is entanglement needed for quantum computation? *Phys. Rev. Lett.* **87**, 047901 (2001).
- [5] C. H. Bennett, G. Brassard, C. Crépeau, R. Jozsa, A. Peres, and W. K. Wootters, Teleporting an unknown quantum state via dual classical and Einstein-Podolsky-Rosen channels, *Phys. Rev. Lett.* **70**, 1895 (1993).
- [6] V. Giovannetti, S. Lloyd, and L. Maccone, Advances in quantum metrology, *Nat. Photonics* **5**, 222 (2011).
- [7] Y. Guo, Partial-norm of entanglement: entanglement monotones that are not monogamous, *New J. Phys.* **25**, 083047 (2023).
- [8] W. K. Wootters, Entanglement of formation of an arbitrary state of two qubits, *Phys. Rev. Lett.* **80**, 2245 (1998).
- [9] C. H. Bennett, H. J. Bernstein, S. Popescu, and B. Schumacher, Concentrating partial entanglement by local operations, *Phys. Rev. A* **53**, 2046 (1996).
- [10] H. He and G. Vidal, Disentangling theorem and monogamy for entanglement negativity, *Phys. Rev. A* **91**, 012339 (2015).
- [11] F. Mintert, M. Kus, and A. Buchleitner, Concurrence of mixed multipartite quantum states, *Phys. Rev. Lett.* **95**, 260502 (2005).
- [12] W. Dür, G. Vidal, and J. I. Cirac, Three qubits can be entangled in two inequivalent ways, *Phys. Rev. A* **62**, 062314 (2000).
- [13] S. Xie, D. Younis, Y. Mei, and J. H. Eberly, Multipartite Entanglement: A Journey through Geometry, *Entropy* **26**, 217 (2024).
- [14] Y. Guo, Y. P. Jia, X. P. Li, and L. Z. Huang, Genuine multipartite entanglement measure, *J. Phys. A* **55**, 145303 (2022).
- [15] Z. H. Ma, Z. H. Chen, J. L. Chen, C. Spengler, A. Gabriel, and M. Huber, Measure of genuine multipartite entanglement with computable lower bounds, *Phys. Rev. A* **83**, 062325 (2011).
- [16] Z. X. Jin, Y. H. Tao, Y. T. Gui, S. M. Fei, X. Li-Jost, and C. F. Qiao, Concurrence triangle induced genuine multipartite entanglement measure, *Results Phys.* **44**, 106155 (2023).
- [17] J. Eisert and H. J. Briegel, Schmidt measure as a tool for quantifying multiparticle entanglement, *Phys. Rev. A* **64**, 022306 (2001).
- [18] D. A. Meyer and N. R. Wallach, Global entanglement in multiparticle systems, *J. Math. Phys.* **43**, 4273 (2002).
- [19] V. Coffman, J. Kundu, and W. K. Wootters, Distributed entanglement, *Phys. Rev. A* **61**, 052306 (2000).
- [20] B. Jungnitsch, T. Moroder, and O. Gühne, Taming multiparticle entanglement, *Phys. Rev. Lett.* **106**, 190502 (2011).
- [21] S. B. Xie and J. H. Eberly, Triangle measure of tripartite entanglement, *Phys. Rev. Lett.* **127**, 040403 (2021).
- [22] X. Z. Ge, L. J. Liu, and S. M. Cheng, Tripartite entanglement measure under local operations and classical communication, *Phys. Rev. A* **107**, 032405 (2023).
- [23] X. Ge, Y. Wang, Y. Xiang, G. Zhang, L. Liu, L. Li, and S. Cheng, Faithful geometric measures for genuine tripartite entanglement, *Phys. Rev. A* **110**, L010402 (2024).
- [24] R. Uola, A. C. S. Costa, H. Chau Nguyen, and O. Gühne, Quantum steering, *Rev. Mod. Phys.* **92**, 015001 (2020).
- [25] R. Gallego and L. Aolita, Resource theory of steering, *Phys. Rev. X* **5**, 041008 (2015).
- [26] Y. Xiang, S. Cheng, Q. Gong, Z. Ficek, and Q. He, Quantum steering: Practical challenges and future directions, *PRX Quantum* **3**, 030102 (2022).
- [27] E. G. Cavalcanti, Q. Y. He, M. D. Reid, and H. M. Wiseman, Unified criteria for multipartite quantum nonlocality, *Phys. Rev. A* **84**, 032115 (2011).
- [28] Q. Y. He and M. D. Reid, Genuine multipartite einstein-podolsky-rosen steering, *Phys. Rev. Lett.* **111**, 250403 (2013).
- [29] C. M. Li, K. Chen, Y. N. Chen, Q. Zhang, Y. A. Chen, and J. W. Pan, Genuine high-order Einstein-Podolsky-Rosen steering, *Phys. Rev. Lett.* **115**, 010402 (2015).
- [30] M. D. Reid, Monogamy inequalities for the Einstein-Podolsky-Rosen paradox and quantum steering, *Phys. Rev. A* **88**, 062108 (2013).
- [31] L. Lami, C. Hirche, G. Adesso, and A. Winter, Schur complement inequalities for covariance matrices and monogamy of quantum correlations, *Phys. Rev. Lett.* **117**, 220502 (2016).
- [32] Y. Xiang, I. Kogias, G. Adesso, and Q. He, Multipartite Gaussian steering: Monogamy constraints and quantum cryptography applications, *Phys. Rev. A* **95**, 010101(R) (2017).
- [33] X. N. Zhu and S. M. Fei, Generalized monogamy relations of concurrence for N-qubit systems, *Phys. Rev. A* **92**, 062345 (2015).
- [34] Q. C. Song, T. J. Baker, and H. M. Wiseman, Shareability of steering in 2-producible states, *Phys. Rev. A* **108**, 012216 (2023).
- [35] S. Gupta, A. G. Maity, D. Das, A. Roy, and A. S. Majumdar, Genuine Einstein-Podolsky-Rosen steering of three-qubit states by multiple sequential observers, *Phys. Rev. A* **103**, 022421 (2021).
- [36] B. Paul and K. Mukherjee, Shareability of quantum steering and its relation with entanglement, *Phys. Rev. A* **102**, 052209 (2020).
- [37] Z. Y. Hao, K. Sun, Y. Wang, Z. H. Liu, M. Yang, J. S. Xu, C. F. Li, and G. C. Guo, Demonstrating shareability of multipartite Einstein-Podolsky-Rosen steering, *Phys. Rev. Lett.* **128**, 120402 (2022).
- [38] M. Wang, Y. Xiang, H. Kang, D. Han, Y. Liu, Q. He, Q. Gong, X. Su, and K. Peng, Deterministic distribution of multipartite entanglement and steering in a quantum network by separable states, *Phys. Rev. Lett.* **125**, 260506 (2020).
- [39] S. Armstrong, M. Wang, R. Y. Teh, Q. Gong, Q. He, J. Janousek, H.-A. Bachor, M. D. Reid, and P. K. Lam, Multipartite Einstein-Podolsky-Rosen steering and genuine tripartite entanglement with optical networks, *Nat. Phys.* **11**, 167 (2015).
- [40] A. C. S. Costa and R. M. Angelo, Quantification of Einstein-Podolsky-Rosen steering for two-qubit states, *Phys. Rev. A* **93**, 020103(R) (2016).
- [41] K. J. Resch, P. Walther, and A. Zeilinger, Full characterization of a three-photon Greenberger-Horne-Zeilinger state using quantum state tomography, *Phys. Rev. Lett.* **94**, 070402 (2005).
- [42] J. Miguel-Ramiro, F. Riera-Sabat, and W. Dur, Quantum Repeater for W States, *PRX Quantum* **4**, 040323 (2023).
- [43] Y. S. Weinstein, Tripartite entanglement witnesses and entanglement sudden death, *Phys. Rev. A* **79**, 012318 (2009).

- [44] S. Gupta, Genuine three qubit Einstein–Podolsky–Rosen steering under decoherence: revealing hidden genuine steerability via pre-processing, *Quant. Inf. Process.* **22**, 49 (2023).
- [45] D. T. Pegg, L. S. Phillips, and S. M. Barnett, Optical state truncation by projection synthesis, *Phys. Rev. Lett.* **81**, 1604 (1998).
- [46] S. M. Barnett and D. T. Pegg, Optical state truncation, *Phys. Rev. A* **60**, 4965 (1999).
- [47] A. Miranowicz, J. Kadlec, K. Bartkiewicz, A. Cernoch, Y. N. Chen, K. Lemr, and F. Nori, Quantifying nonclassicality of vacuum–one-photon superpositions via potentials for Bell nonlocality, quantum steering, and entanglement, [arXiv:2309.12930](https://arxiv.org/abs/2309.12930).
- [48] S. L. Braunstein, Quantum error correction for communication with linear optics, *Nature (London)* **394**, 47 (1998).
- [49] P. van Loock and S. L. Braunstein, Multipartite entanglement for continuous variables: A quantum teleportation network, *Phys. Rev. Lett.* **84**, 3482 (2000).
- [50] S. B. Xie and J. H. Eberly, Multipartite entanglement and geometry, *Proc. SPIE* **12633**, 1263306 (2023).
- [51] A. Ekert and P. L. Knight, Entangled quantum systems and the Schmidt decomposition, *Am. J. Phys.* **63**, 415 (1995).
- [52] A. Acín, A. Andrianov, L. Costa, E. Jane, J. I. Latorre, and R. Tarrach, Generalized schmidt decomposition and classification of three-quantum-bit states, *Phys. Rev. Lett.* **85**, 1560 (2000).
- [53] M. Walter, B. Doran, D. Gross, and M. Christandl, Entanglement Polytopes: Multiparticle Entanglement from Single-Particle Information, *Science* **340**, 1205 (2013).
- [54] X. F. Qian, M. A. Alonso, and J. H. Eberly, Entanglement polygon inequality in qubit systems, *New J. Phys.* **20**, 063012 (2018).
- [55] Y. Z. Zhen, Y. L. Zheng, W. F. Cao, L. Li, Z. B. Chen, N. L. Liu, and K. Chen, Certifying Einstein-Podolsky-Rosen steering via the local uncertainty principle, *Phys. Rev. A* **93**, 012108 (2016).
- [56] M. S. Winnel, N. Hosseini-dehaj, and T. C. Ralph, Generalized quantum scissors for noiseless linear amplification, *Phys. Rev. A* **102**, 063715 (2020).
- [57] J. J. Guanzon, M. S. Winnel, A. P. Lund, and T. C. Ralph, Ideal quantum teleamplification up to a selected energy cutoff using linear optics, *Phys. Rev. Lett.* **128**, 160501 (2022).
- [58] J. J. Guanzon, M. S. Winnel, D. Singh, A. P. Lund, and T. C. Ralph, Saturating the maximum success probability bound for noiseless linear amplification using linear optics, *PRX Quantum* **5**, 020359 (2024).
- [59] I. Frerot, M. Fadel, and M. Lewenstein, Probing quantum correlations in many-body systems: a review of scalable methods, *Rep. Prog. Phys.* **86**, 114001 (2023).
- [60] N. Friis, G. Vitagliano, M. Malik, and Marcus Huber, Entanglement certification from theory to experiment, *Nat. Rev. Phys.* **1**, 72 (2019).
- [61] L. Knips, C. Schwemmer, N. Klein, M. Wiesniak, and H. Weinfurter, Multipartite entanglement detection with minimal effort, *Phys. Rev. Lett.* **117**, 210504 (2016).
- [62] Y. Li, Y. Xiang, X.D. Yu, H.C. Nguyen, O. Gühne, and Q. He, Randomness certification from multipartite quantum steering for arbitrary dimensional systems, *Phys. Rev. Lett.* **132**, 080201 (2024).
- [63] K. N. Huynh-Vu, L. H. Zaw, and V. Scarani, Certification of genuine multipartite entanglement in spin ensembles with measurements of total angular momentum, *Phys. Rev. A* **109**, 042402 (2024).
- [64] O. Gühne, E. Haapasalo, T. Kraft, J. P. Pellonpää, and R. Uola, Colloquium: Incompatible measurements in quantum information science, *Rev. Mod. Phys.* **95**, 011003 (2023).